SUPPLEMENTAL DATA

Detecting Material State Changes in the Nucleolus by Label-free Digital Holographic Microscopy

Christiane Zorbas[1], Aynur Soenmez[1], Jean Léger[2], Christophe De Vleeschouwer[2], and Denis L.J. Lafontaine[1,3*]

[1]RNA Molecular Biology, Fonds de la Recherche Scientifique (F.R.S./FNRS), Université libre de Bruxelles (ULB), Biopark campus, B-6041 Gosselies, Belgium

[2]ICTEAM-ELEN, Fonds de la Recherche Scientifique (F.R.S./FNRS), UCLouvain, B-1348 Louvain-la-Neuve, Belgium

[3]Centre for Microscopy and Molecular Imaging (CMMI), Université libre de Bruxelles (ULB), Biopark campus, B-6041 Gosselies, Belgium

[*]To whom correspondence should be addressed: denis.lafontaine@ulb.be

RUNNING TITLE Digital Holographic Detection of Nucleoli

KEYWORDS Digital Holographic Microscopy; Nucleolus; Ribosome; Liquid-Liquid Phase Separation (LLPS); Biomolecular condensate; Cancer

EXPANDED VIEW FIGURE LEGENDS

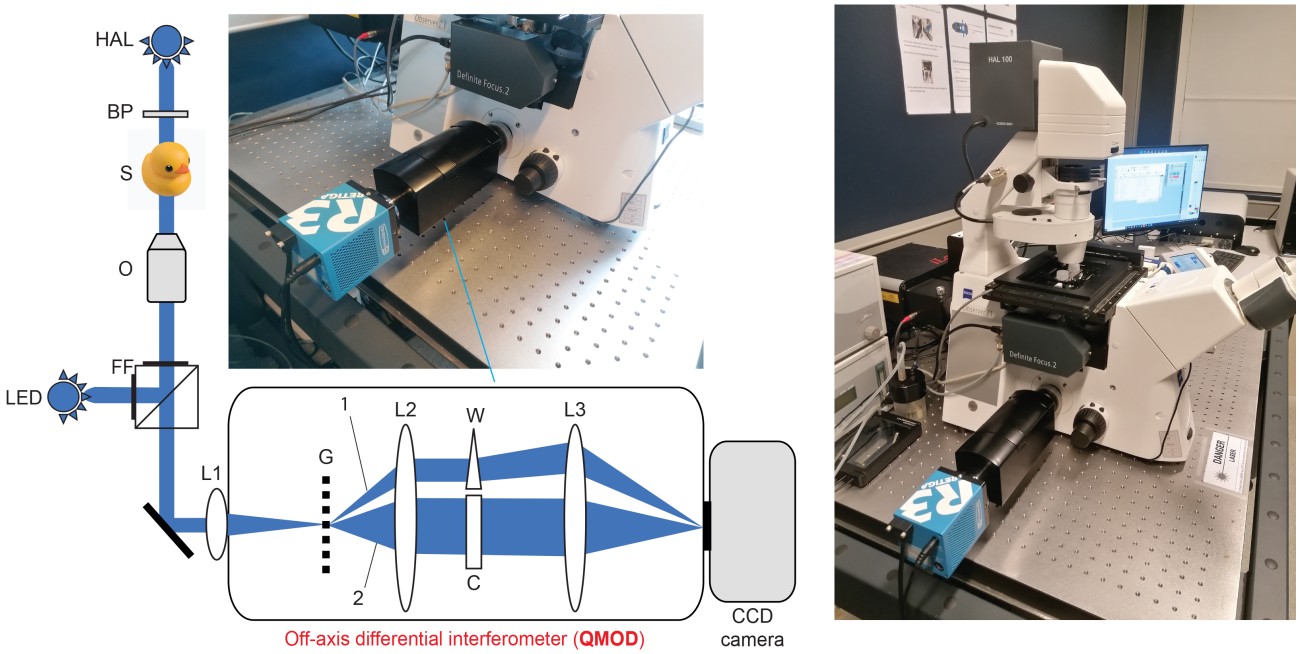

Figure EV1. Off-axis differential interferometer (QMOD) setup used in this work. Description of the beam path and microscope configuration used. The diagram illustrates the detailed beam path in our QMOD setup. A purposely built versatile "plug in" DHM adapter (QMOD, developed together with Ovizio s.a.) was connected between the lateral port of a Zeiss inverted microscope and a Retiga R3 camera (Qimaging) used for imaging the DHM phase and all fluorescence channels. The camera was driven from the MetaXpress (Molecular Devices) environment. Images were processed with OsOne (Ovizio). Digital holograms were recorded with an incoherent light source (**HAL** lamp) on an inverted microscope adjusted for proper Köhler illumination and coupled to a QMOD interferometer and CCD camera. A bandpass filter (**BP**) was used to increase the coherence of the light and obtain the partial coherence required for holography. The image forming light rays passing through the specimen (**S**) were captured with the microscope objective (**O**) and directed from microscope lens **L1** to the QMOD interferometer. In the QMOD, a diffraction grating **G** induced splitting of the incident light beam into a diffracted beam (**1**, reference) and a non-diffracted light beam (**2**, object beam). A second lens (**L2**) placed at focal distance from the grating G reshaped both the diffracted and non-diffracted beams into beams parallel to the optical axis. A wedge (**W**) inserted in the optical path of the object beam induced a slight shift of the images produced by the diffracted and non-diffracted light beams. **C** is a compensating optical module placed in the optical path of the non-diffracted light beam to compensate for the light shift introduced by W in the diffracted beam. The diffracted beam is then recombined with the object beam and focalized by means of objective lens **L3** on the recording plane of a CCD camera, where the hologram is recorded. LED, illumination; FF, fluorescent filter cube. Fluorescence imaging: excitation illumination is emitted by a light-emitting diode (**LED**) and is directed to the sample (**S**) through a fluorescence filter cube (**FF**). Fluorescence emission by the specimen is collected by the objective, passes through the filter cube and **L1**, enters the QMOD, and finally reaches the CCD camera.

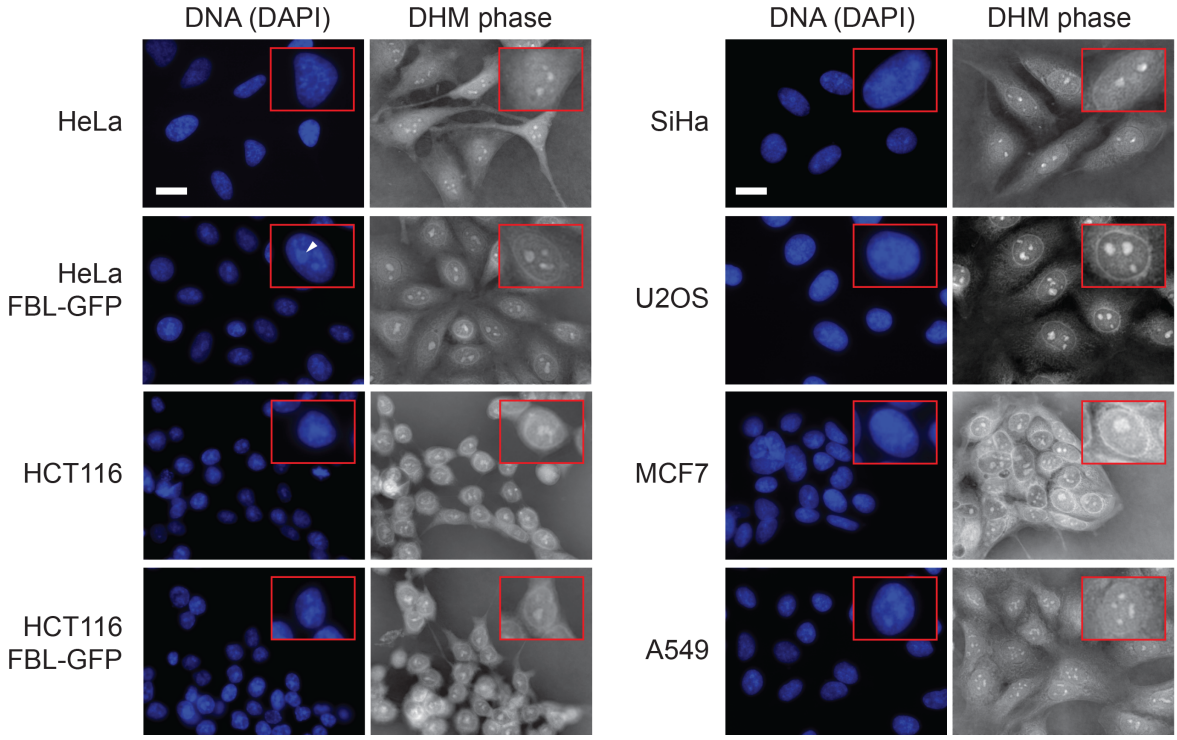

Figure EV2. DHM detection of the nucleolus in cell lines of various origins.
The various cell lines indicated were observed by correlative fluorescence-DHM. Cells were stained with DAPI. An example of a perinucleolar chromatin ring, lining the nucleolus, is highlighted with an arrowhead in the HeLa-FBL-GFP panel for reference (see Fig 2B for details). Scale bar, 20 µm.

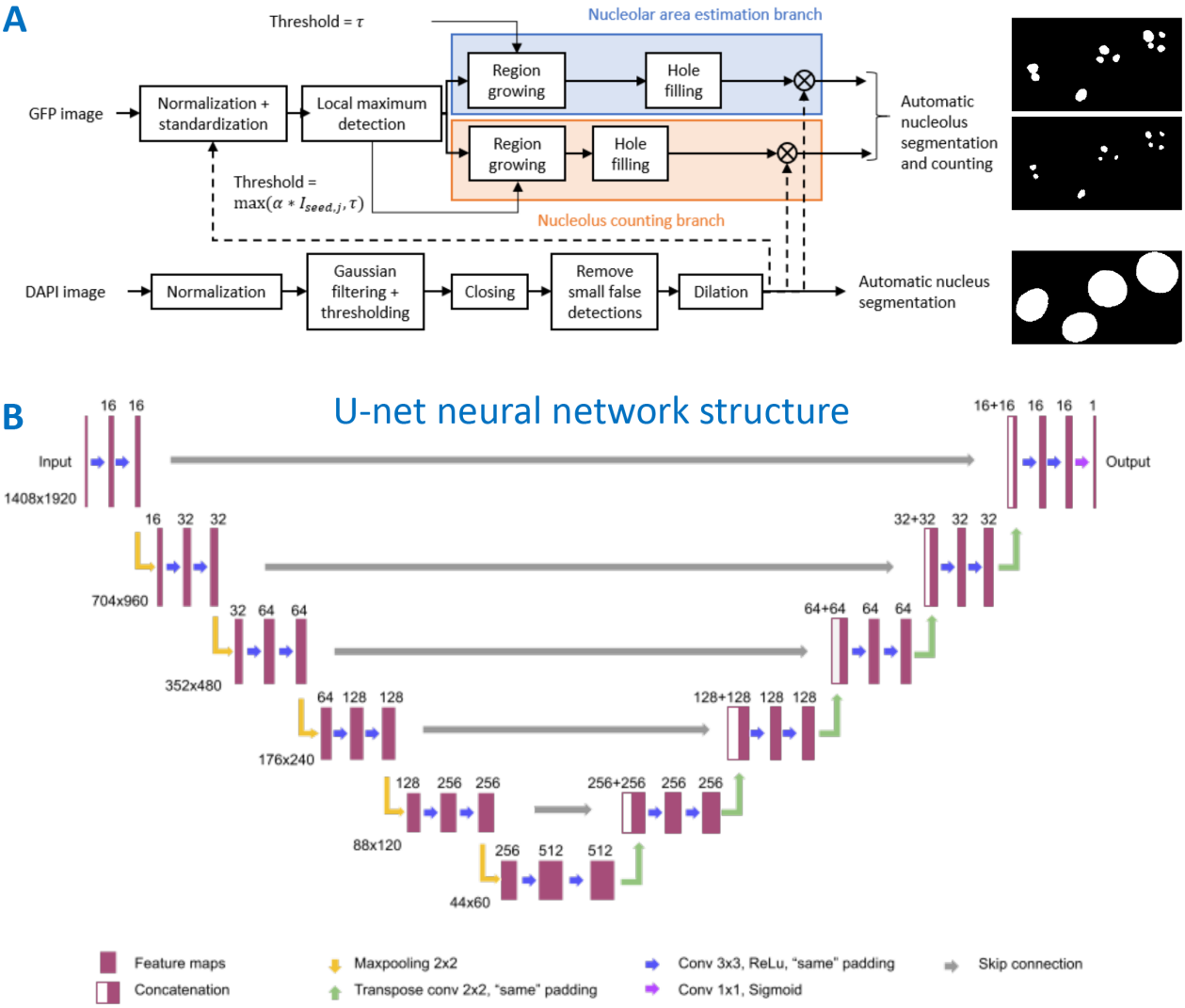

Figure EV3. Image processing pipeline.

A Segmentation pipeline of fluorescence images. The dynamic range of the GFP and DAPI images was normalized to $[0, 1]$. GFP images were further standardized image-wise. Seeds were automatically positioned on the pixels with local maximum intensity in the GFP images. Starting from those seeds, region-growing algorithms were used with a constant threshold for nucleolus area estimation and an adaptive threshold for counting. $I_{seed,j}$ is the pixel intensity of seed j, τ the constant, and α a scalar between

0 and 1. Unrealistic holes remaining in segmented nucleolar masks were filled in a postprocessing step. After normalization, the DAPI images were filtered with a Gaussian kernel and an adaptive threshold was applied. The threshold was adapted for every DAPI image on the basis of the background and foreground (i.e., nucleus) pixel intensity distributions. Further postprocessing of the segmented nuclear masks included a morphological closing operation, removal of false detections, and a final morphological dilation operation. The symbol $\otimes$ denotes pixel-wise multiplication between binary masks to ensure that only nucleolar pixels contained within the nuclear area were considered to be *bona fide* nucleoli. The binary mask output of fluorescence image segmentation is illustrated (insets).
B Architecture of the 2D U-net convolutional neural network. Convolution operators are filters that extract image patterns useful for segmentation. The analysis path (left part) allows capturing context, whereas the synthesis path (right path) and skip connections allow retrieving high output resolution.
C Segmentation pipeline of DHM images. Two neural networks were trained, one with binary masks of nucleoli obtained by segmentation of the GFP images, the other with binary masks of nuclei obtained by segmentation of the DAPI channel. The binary mask output of DHM image segmentation is illustrated (insets).

A

Number of nucleoli per cell	Number of cells	Measured nucleolar area (µm²)	Predicted nucleolar area (µm²)
1	238	22.62 ± 9.27	22.62
2	473	22.56 ± 7.48	≤ 28.49
3	331	22.72 ± 9.03	≤ 32.62
4	129	23.95 ± 13.10	≤ 35.91
5	25	31.21 ± 12.72	≤ 38.68
6	6	45.78 ± 9.67	≤ 41.10
7	4	48.93 ± 31.29	≤ 43.27

B

Counted on GFP images:

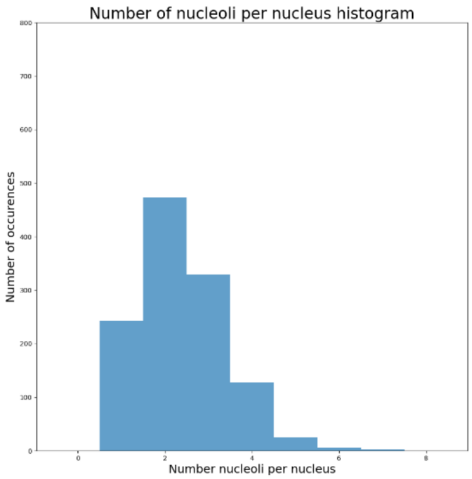

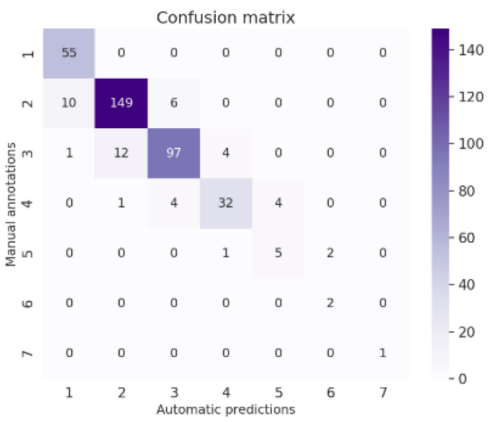

Counted on DHM images:

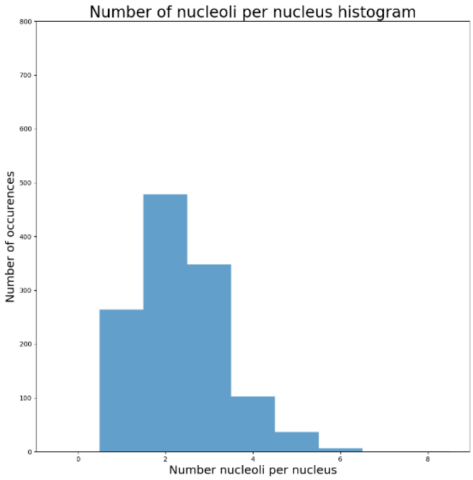

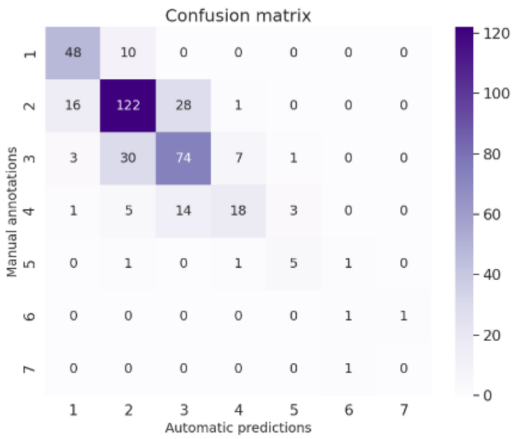

C

Number of nucleoli per cell	Fluorescence / Thresholding			DHM phase / Neural network		
	Sensitivity	Specificity	Precision	Sensitivity	Specificity	Precision
$n = 1$	1	0.97	0.83	0.83	0.94	0.71
$n = 2$	0.90	0.94	0.92	0.73	0.80	0.73
$n = 3$	0.85	0.96	0.91	0.64	0.85	0.64
$n = 4$	0.78	0.99	0.86	0.44	0.98	0.67

Figure EV4: Benchmarking of data analysis.

A Conservation of the mean nucleolar area according to the number of nucleoli per cell. The predicted value is a theoretical upper limit, considering that the area occupied by a single spherical nucleolus is multiplied by $N^{1/3}$ when the nucleolus is partitioned into N identical spheres.

B Histogram representing the number of nucleoli per nucleus automatically counted on the fluorescence images (left) and DHM images (right). Confusion matrices assessing automatic counting of nucleoli on the fluorescence images. The matrices compare the manual and automatic counts of nucleoli on 25 images. Element (i,j) in the confusion matrix is the number of nuclei with i nucleoli for which the algorithm counted j nucleoli. The elements on the main matrix diagonal were correctly counted**.** The lower the total value of elements outside the main diagonal, the better the counting.

C Sensitivity (true positive rate), specificity (true negative rate), and precision (proportion of properly classified cells) of the cell classification based on their number of nucleoli. Sensitivity provides the probability of counting n nucleoli amongst cells truly displaying n nucleoli. Specificity provides the probability of not counting n nucleoli amongst cells displaying n nucleoli. Precision provides the proportion of cells correctly classified. The closer the sensitivity, specificity, and precision are to 1, the better the approach.

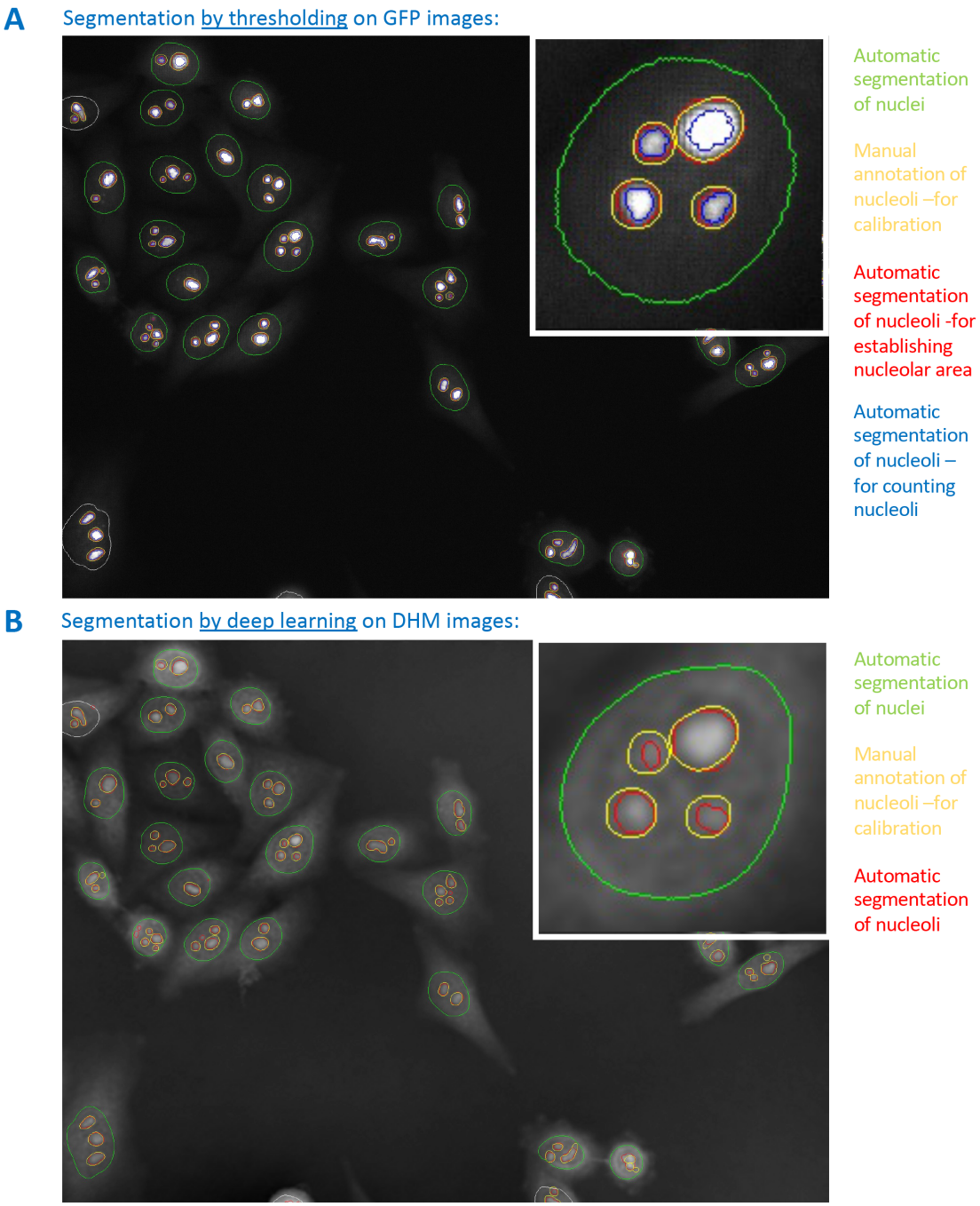

Figure EV5. Comparison of segmentation of the GFP signal by thresholding and of the DHM signal by deep learning.

A Segmentation of the GFP signal by thresholding. Red, automatic segmentation of nucleoli on GFP images by 'region growing', for computing the nucleolar area; blue: automatic segmentation of nucleoli by 'region growing', for counting; yellow: manual annotation for validation of the nucleolus counting algorithm; green: automatic segmentation of the nuclei on GFP images by thresholding; gray, eliminated cells (image edges, clustered cells, etc.).

B Segmentation of the DHM signal by deep learning. Red, automatic segmentation of nucleoli on DHM images by deep learning (for counting, area computation, and nucleolar optical thickness computation); green, automatic segmentation of the nuclei on DHM images by deep learning; yellow, same as in panel A.

SUPPLEMENTAL MOVIES

Movie 1. DHM live-cell imaging through mitosis.

Representative live imaging of HeLa-FBL-GFP cells. Cells were imaged with a 20x objective over a 12-h period in 1-min intervals in the DHM and fluorescence modes.

Movie 2. DHM live-cell imaging upon roscovitine treatment.

Live imaging of HeLa-FBL-GFP cells treated with 50 μM roscovitine in 0.1% DMSO. The red arrow indicates the first detectable changes in nucleolar morphology. Cells were imaged with a 20x objective over a 3-h period in 30-s intervals in the DHM and fluorescence modes.